

# Lifetime-Weighted FCS and 2D FLCS: Advanced Application of Time-Tagged TCSPC

Kunihiko Ishii, Takuhiro Otsu, and Tahei Tahara

**Abstract** Time-tagged TCSPC (time-correlated single photon counting) is a special acquisition mode of TCSPC with which one determines not only the excitation-emission delay time of detected photons but also their arrival times measured from the start of the experiment. Time-tagged TCSPC enables us to examine slow fluctuation of fluorescence lifetimes, which is particularly important in the study of heterogeneous or fluctuating systems at the single-molecule level. In this chapter, we describe recent development of new methods using time-tagged TCSPC, aiming at showing their high potential in studying dynamics of complex systems. We depict two closely related methods based on fluorescence correlation spectroscopy (FCS), i.e., lifetime-weighted FCS and two-dimensional fluorescence lifetime correlation spectroscopy (2D FLCS). These methods enable us to quantify fluorescence lifetime fluctuations on the microsecond timescale. Showing examples including the study of a biological macromolecule, we demonstrate the usefulness of these two methods in real applications. In addition, we present another application of time-tagged TCSPC, which analyzes photon interval time for characterizing timing instability of photon detectors.

**Keywords** Biological macromolecules · Fluorescence correlation spectroscopy · Fluorescence lifetime · Microsecond dynamics · Time-tagged TCSPC

## Contents

1	Introduction .....	112
2	Lifetime-Weighted Fluorescence Correlation Spectroscopy .....	114
3	Two-Dimensional Fluorescence Lifetime Correlation Spectroscopy (2D FLCS) .....	116

---

K. Ishii, T. Otsu, and T. Tahara (✉)

Molecular Spectroscopy Laboratory, RIKEN, 2-1 Hirosawa, Wako, Saitama 351-0198, Japan  
e-mail: [tahei@riken.jp](mailto:tahei@riken.jp)

3.1	Constructing Two-Dimensional Correlation Map .....	116
3.2	Background Subtraction .....	119
3.3	Inverse Laplace Transform and Decomposition into Multiple Species .....	120
3.4	Application: DNA Dynamics .....	123
4	Photon Interval Analysis .....	125
5	Concluding Remarks .....	127
	References .....	127

## 1 Introduction

Time-correlated single photon counting (TCSPC) is a sensitive method for the measurement of fluorescence lifetime with a time resolution of tens to hundreds of picoseconds. A typical TCSPC setup consists of a pulsed excitation source, a photon detector having a short response time, and an electronic circuit which can precisely determine the delay time between the excitation pulse and the photon signal in the unit of TCSPC channel number (“microtime,” Fig. 1). After accumulating sufficient number of fluorescence photons, a fluorescence decay curve is built as a histogram of the obtained microtimes. The characteristic fluorescence lifetime of the sample molecule is evaluated from the fluorescence decay curve, typically by fitting analysis using exponential functions.

In ordinary TCSPC experiments, only the microtimes of detected photons are recorded for building the ensemble-averaged histogram, while information of the temporal fluctuation of the microtime in a slower timescale (microseconds to seconds) is discarded. On the other hand, in time-tagged TCSPC [1], one keeps a record of the absolute arrival time of individual photons measured from the start of the experiment (“time tag” or “macrotime,” Fig. 1). Combined use of the microtime and macrotime information facilitates simultaneous measurements of fluorescence lifetime and fluorescence intensity fluctuations. Moreover, this acquisition mode of fluorescence photons allows us to analyze the correlation of the microtime and macrotime, which in fact provides information about the fluctuation of fluorescence lifetimes on the microsecond to second timescale. Such fluctuation of the fluorescence lifetime is essential in fluorescence measurements at the single-molecule level, where the fluctuation is caused by conformational dynamics of the molecule. In order to access rich information contained in the fluctuation of fluorescence lifetimes in single-molecule experiments, a reliable, convenient, and versatile method for analyzing time-tagged TCSPC data is critically important.

To date, several methods have been reported to analyze time-tagged TCSPC data. For example, burst-integrated fluorescence lifetime (BIFL) [2] and fluorescence intensity and lifetime distribution analysis (FILDA) [3] are single-molecule-based techniques with which one examines distribution of fluorescence lifetimes by evaluating the mean fluorescence lifetime in short binning windows and analyzing its statistics. These methods can be used to detect distribution of the fluorescence lifetime in static multi-component systems. However, they are not suitable for

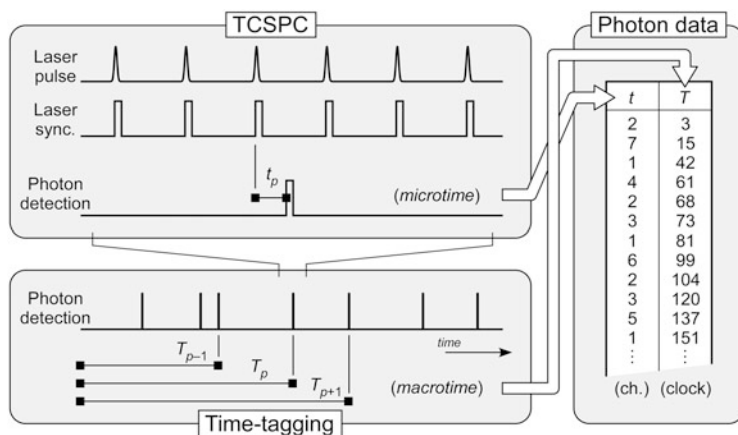


**Fig. 1** Schematic description of a time-tagged TCSPC data. For each detected photon, microtime ( $t$ ) and macrotime ( $T$ ) are measured with the TCSPC module. Photon data is a combined list of microtimes and macrotimes of detected photons sorted with the macrotime values

dynamic systems that involve rapid lifetime fluctuations, because the time binning limits the time resolution to the bin width.

Fluorescence correlation spectroscopy (FCS) based techniques treat time-tagged TCSPC data with a binning-free (photon-by-photon) manner [4]. Therefore, they allow us to study fluorescence lifetime fluctuations with a time resolution down to tens of nanoseconds. Fluorescence lifetime correlation spectroscopy (FLCS) [5–8] is a useful technique when one has information about the fluorescence decay of each species in advance. In this case, FLCS utilizes the microtime information of each detected photon to infer the source of the photon, i.e., the species from which the photon is emitted. By comparing the observed microtimes with the fluorescence decay curve of each species (reference), FLCS can determine the auto- and cross-correlations of relevant species in a species-selective manner. Nevertheless, FLCS is not applicable in case that we do not have information about the fluorescence lifetime of the component. Therefore, one needs a new “reference-free” method for studying conformational dynamics of macromolecules where unknown intermediate states may appear.

In this chapter, we describe our recent effort to develop reference-free methods to study conformational dynamics of macromolecules using time-tagged TCSPC. Lifetime-weighted FCS [9] is a simple reference-free method to detect inhomogeneity in the sample through fluorescence lifetime fluctuations. This method is used for finding inhomogeneity in the sample and/or for “the first examination” of the timescale of the conformational dynamics of macromolecules. Two-dimensional fluorescence lifetime correlation spectroscopy (2D FLCS) [10–12] is a recently developed versatile reference-free method which analyzes time-tagged TCSPC data by building two-dimensional correlation maps. 2D FLCS is particularly useful for investigating complex dynamics of unknown systems in a visually comprehensible

manner. At last, we describe another type of application of time-tagged TCSPC. It is shown that the photon interval analysis on the time-tagged TCSPC data can solve a long-standing problem of timing instability of photon detectors [13].

## 2 Lifetime-Weighted Fluorescence Correlation Spectroscopy

Usually, FCS experiments are performed by observing the correlation function of time-dependent fluorescence intensity,  $I(T)$  [14]:

$$G_1(\Delta T) = \frac{\langle I(T)I(T + \Delta T) \rangle}{\langle I(T) \rangle^2}, \quad (1)$$

where  $\Delta T$  is the correlation lag time and angle brackets denote ensemble averaging. This quantity is evaluated photon-by-photon using time-tagged photon data as

$$G_1(\Delta T) = \frac{\sum_{p=1}^N \sum_{q=1}^N \begin{cases} 1 & \Delta T - \Delta\Delta T/2 < T_q - T_p < \Delta T + \Delta\Delta T/2 \\ 0 & \text{otherwise} \end{cases}}{N^2 T_{\max}^{-2} \cdot (T_{\max} - \Delta T) \cdot \Delta\Delta T}. \quad (2)$$

Here,  $T_{p(q)}$  is the macrotime of  $p(q)$ -th photon,  $N$  is the total number of detected photons,  $\Delta\Delta T$  is an arbitrary window size, and  $T_{\max}$  is the measurement time. In this definition, one searches for all possible pairings of photons in the time-tagged TCSPC data which satisfy the condition that the time lag between the pair is  $\Delta T$  (Fig. 2a). The denominator of Eq. (2) is the normalization factor that is chosen such that  $G_1(\Delta T)$  becomes unity when there is no intensity correlation.  $G_1(\Delta T)$  characterizes the fluctuations of fluorescence intensity.

If one incorporates the microtime data obtained by time-tagged TCSPC to FCS, one can investigate fluorescence lifetime fluctuations. The simplest way is to replace “1” in the numerator of Eq. (2) with the product of microtimes ( $t$ ) of photons  $p$  and  $q$  (Fig. 2a) [9]:

$$G_L(\Delta T) = \frac{\sum_{p=1}^N \sum_{q=1}^N \begin{cases} t_p t_q & \Delta T - \Delta\Delta T/2 < T_q - T_p < \Delta T + \Delta\Delta T/2 \\ 0 & \text{otherwise} \end{cases}}{\bar{t}^2 N^2 T_{\max}^{-2} \cdot (T_{\max} - \Delta T) \cdot \Delta\Delta T}, \quad (3)$$

where  $\bar{t} = \sum_{p=1}^N t_p / N$  is the ensemble-averaged mean fluorescence lifetime. Equation (3) is equivalent to

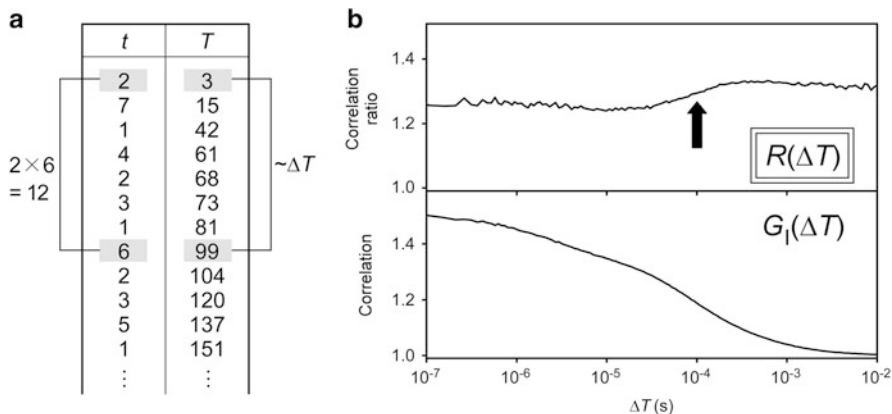


**Fig. 2** (a) Correlation calculation from time-tagged TCSPC data. Photon pairs with the interval of  $\Delta T$  are looked up in the photon data and their occurrences are counted. In the lifetime-weighted FCS, the counting is weighted with the product of corresponding microtimes. (b) The result of lifetime-weighted FCS measurements of a DNA hairpin. *Top*: correlation ratio defined in Eq. (5). The *arrow* indicates a transition of the correlation ratio. *Bottom*: ordinary fluorescence intensity correlation

$$G_L(\Delta T) = \frac{\langle t(T)I(T)t(T + \Delta T)I(T + \Delta T) \rangle}{\langle t(T)I(T) \rangle^2}, \quad (4)$$

where  $t(T)$  is the fluorescence lifetime at the macroscopic time  $T$ . The right-hand side of this equation can be interpreted as the correlation function of the “lifetime-weighted” fluorescence intensity. Note that, although it may seem counterintuitive, Eq. (3) is not the correlation function of the fluorescence lifetime itself, i.e.,  $\langle t(T)t(T + \Delta T) \rangle / \langle t(T) \rangle^2$ . The intensity factor  $I(T)$  appears in Eq. (4) because the photon-by-photon evaluation of a correlation function is inevitably influenced by the fluctuation of fluorescence intensity. Therefore, more photons are sampled from the time region where the fluorescence intensity is higher.

For separating the lifetime fluctuation from the intensity fluctuation, one can employ the ratio of the lifetime-weighted fluorescence correlation (Eq. (3)) to the ordinary intensity correlation (Eq. (2)) [9],

$$R(\Delta T) = \frac{G_L(\Delta T) - 1}{G_I(\Delta T) - 1}. \quad (5)$$

By canceling the correlation amplitude due to intensity fluctuations as Eq. (5), one can examine the extent and timescale of the fluctuation of the fluorescence lifetime. If the system is homogeneous,  $R(\Delta T)$  becomes unity; In contrast, if the system consists of multiple species having different fluorescence lifetimes,  $R(\Delta T)$  takes a value deviated from unity. A dynamic process such as conformational dynamics usually induces an interconversion between species having different fluorescence lifetimes, and hence it causes a change of  $R(\Delta T)$ . Importantly, as long as there is no

variation in the diffusion behavior of the molecules in the sample,  $R(\Delta T)$  defined as Eq. (5) is free from the diffusion effect and reports only intramolecular dynamics that causes fluctuations of the fluorescence lifetime. This feature is particularly important when one studies conformational dynamics of macromolecules in the micro to millisecond time region.

Figure 2b shows the  $R(\Delta T)$  curve of a single-stranded DNA forming a hairpin structure (6-FAM-5'-TTTAACC(T)<sub>18</sub>GGTT-3'-TAMRA) [12]. The DNA sample is labeled with two fluorophores that constitute a Förster resonance energy transfer (FRET) pair. The FRET efficiency from the donor (FAM) to the acceptor (TAMRA) increases drastically upon formation of the hairpin structure. Therefore, one can study the formation-dissociation dynamics of the DNA hairpin through monitoring the FRET efficiency. The FRET efficiency,  $E$ , is represented by the fluorescence lifetime of the donor,  $\tau_D$ , as

$$E = 1 - \frac{\tau_D}{\tau_D^0}, \quad (6)$$

where  $\tau_D^0$  is the intrinsic fluorescence lifetime of the donor in the absence of an acceptor. Therefore, the fluctuation of  $\tau_D$ , which is quantified as  $R(\Delta T)$  of the donor fluorescence, can be used to detect dynamics of the DNA hairpin formation. In Fig. 2b, the  $R(\Delta T)$  curve of the DNA hairpin clearly shows a transition at  $\Delta T \sim 100 \mu\text{s}$ . This is a clear evidence of a dynamics on this timescale which changes the fluorescence lifetime of FAM. In other words, a dynamics that changes the DNA structure is unambiguously detected by lifetime-weighted FCS. It is noteworthy that even though the transition is undoubtedly observed in  $R(\Delta T)$ , the corresponding signature is not apparent in the raw correlation curve ( $G_I(\Delta T)$ ; Fig. 2b) because of coexisting dynamic signals originating from the diffusion and triplet formation.

To summarize, the lifetime-weighted FCS is a simple reference-free application of time-tagged TCSPC data which can be used for detecting inhomogeneity in the sample and the relaxation dynamics of the inhomogeneity through  $R(\Delta T)$ . This method is advantageous over traditional FCS for detecting the dynamics of biological macromolecules. Nevertheless, the lifetime-weighted FCS does not provide detailed knowledge about the system. Specifically, it does not tell about the number of independent species, the fluorescence lifetime of them, and the species involved in the observed dynamics. The next task is to elucidate these details by carefully examining time-tagged TCSPC data, as described in the next section.

### 3 Two-Dimensional Fluorescence Lifetime Correlation Spectroscopy (2D FLCS)

#### 3.1 Constructing Two-Dimensional Correlation Map

Time-tagged TCSPC data consists of lists of the microtimes and macrotimes of detected photons (Fig. 1). In order to thoroughly investigate the correlation pattern

contained in the time-tagged data, one should avoid any loss of information in the analytical process. The best way is to individually evaluate the correlation function for all possible combinations of microtime values,  $\{t^{(i)}, t^{(j)}\}$  [10–12, 15]. In other words, one should use the following form of a correlation function to fully utilize the microtime information in time-tagged data:

$$M_{ij}(\Delta T) = \frac{\sum_{p=1}^N \sum_{q=1}^N \begin{cases} \delta_{t_p t^{(i)}} \delta_{t_q t^{(j)}} & \Delta T - \Delta\Delta T/2 < T_q - T_p < \Delta T + \Delta\Delta T/2 \\ 0 & \text{otherwise} \end{cases}}{(T_{\max} - \Delta T) \cdot \Delta\Delta T} \quad (7)$$

$I(T; t^{(i)})$  is the fluorescence intensity detected by  $i$ th TCSPC channel at macroscopic time  $T$ , and  $\delta_{kl}$  is the Kronecker delta function. For example, if we set  $i = 1$  and  $j = 2$ , Eq. (7) becomes the (unnormalized) cross-correlation function between the fluorescence intensities detected at the first and the second TCSPC channels. By gathering all  $M_{ij}(\Delta T)$  values for various  $\{i, j\}$  combinations together, one obtains a two-dimensional matrix of correlation data,  $\mathbf{M}(\Delta T)$ . Note that if one sums up all the elements of  $\mathbf{M}(\Delta T)$ , one obtains the ordinary (unnormalized) fluorescence intensity correlation, i.e.,  $\sum_i \sum_j M_{ij}(\Delta T) = \langle I(T)I(T + \Delta T) \rangle$ .

In practice, computation of  $\mathbf{M}(\Delta T)$  is done as follows (Fig. 3).

1. An arbitrary timescale of interest and a window size are chosen ( $\Delta T$  and  $\Delta\Delta T$ ).
2. A two-dimensional array of memory space is prepared for storing  $\mathbf{M}(\Delta T)$ . The size of this array is the square of the number of TCSPC channels, e.g.,  $256 \times 256$ .  $\mathbf{M}(\Delta T)$  is initialized by setting zero at all elements of this array.

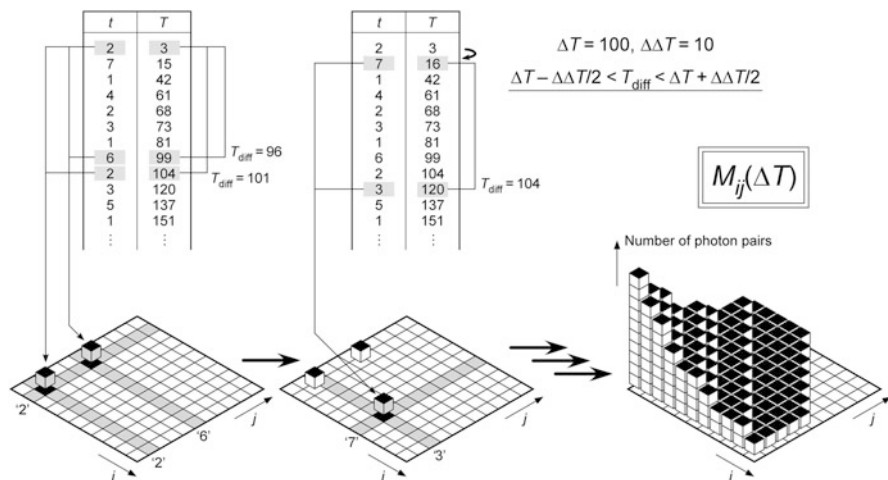


**Fig. 3** Schematic illustration of the procedure for building a two-dimensional correlation map. Here, the correlation timescale ( $\Delta T$ ) and the window size ( $\Delta\Delta T$ ) are set at 100 and 10, respectively. The first part (*left*) represents steps 3–7 and the second part (*center*) represents steps 8–9 (see main text)

3. The macrotime and microtime of the first photon in the time-tagged TCSPC data ( $T_1, t_1$ ) are examined and stored in buffer memory.
4. The macrotime table is scanned to pick up photons that have macrotime values between  $T_1 + \Delta T - \Delta\Delta T/2$  and  $T_1 + \Delta T + \Delta\Delta T/2$ .
5. If a matching photon is found, its microtime is read ( $t_m$ ).
6. The  $\{t_1, t_m\}$  element of  $\mathbf{M}(\Delta T)$  is incremented by 1.
7. Steps 4–6 are repeated to find all matching photons.
8. Step 3 is repeated for the second photon. Its macrotime and microtime ( $T_2, t_2$ ) are examined and stored in buffer memory.
9. Steps 4–7 are repeated for  $T_2$  and  $t_2$ .
10. Steps 8 and 9 are repeated for the rest of photons.

Sometimes FCS experiments are performed in the cross-correlation configuration using two independent detectors in order to avoid artifact due to the afterpulsing effect of the detector [16]. In that case, photons examined in step 3 (or step 8) and in step 4 should be those from different detectors.

Roughly speaking, the physical meaning of the obtained two-dimensional matrix  $\mathbf{M}(\Delta T)$  can be interpreted as follows.

- Elements of  $\mathbf{M}(\Delta T)$  of small  $t^{(i)}, t^{(j)}$  values mainly reflect the autocorrelation of short lifetime species.
- Elements of  $\mathbf{M}(\Delta T)$  of large  $t^{(i)}, t^{(j)}$  values mainly reflect the autocorrelation of long lifetime species.
- Elements of  $\mathbf{M}(\Delta T)$  of small  $t^{(i)}$  and large  $t^{(j)}$  values mainly reflect the cross-correlation between short lifetime species and long lifetime species.

Importantly,  $\mathbf{M}(\Delta T)$  preserves the full information of two-point correlations obtainable from a set of the time-tagged TCSPC data. Therefore, any other analyses of time-tagged TCSPC data can be reinterpreted using  $\mathbf{M}(\Delta T)$ . Such reinterpretation provides a coherent overview of the existing methods, which can lead us to further development of a new analysis. For example, FLCS developed by Enderlein and coworkers [5–8] can be understood in the framework of  $\mathbf{M}(\Delta T)$  as follows. In FLCS, it is assumed that the complete prior knowledge of the fluorescence decay components is available. Then, an observed two-dimensional correlation matrix  $\mathbf{M}(\Delta T)$  is expected to be a sum of auto- and cross-correlations of the known decay curves:

$$M_{ij}(\Delta T) = \sum_{k,l} g_{kl}(\Delta T) I_k(t^{(i)}) I_l(t^{(j)}). \quad (8)$$

Here,  $I_{k(l)}(t)$  is the decay curve of species  $k(l)$  and  $g_{kl}(\Delta T)$  is the correlation between species  $k$  and  $l$  at lag time  $\Delta T$ . FLCS analysis [5–8] is mathematically equivalent to the least mean square fitting of the observed  $\mathbf{M}(\Delta T)$  using Eq. (8), i.e., the fitting using combinations of  $I_k(t)$  and  $I_l(t)$  to determine unknown  $g_{kl}(\Delta T)$ 's. This interpretation of FLCS using a 2D matrix makes it clear that a new analysis is necessary for more general case where one does not have any prior knowledge of



the fluorescence decay components. In such cases, one should simultaneously determine  $I_k(t)$ ,  $I_l(t)$ , and  $g_{kl}(\Delta T)$  from the observed  $\mathbf{M}(\Delta T)$  without any references. In the following, we describe how to achieve this reference-free analysis of  $\mathbf{M}(\Delta T)$ , which is the core of 2D FLCS [10–12].

### 3.2 Background Subtraction

First, one needs to note that a correlation signal obtained in FCS is always accompanied with uncorrelated background due to photon pairs emitted by different molecules that coexist in the observation volume. Emissive background signals, such as solvent Raman scattering, also contribute to the uncorrelated background. One can separate the information of the correlated photons from the uncorrelated background by using  $\mathbf{M}(\Delta T)$  evaluated at a very long  $\Delta T$  [10].

After a sufficiently long lag time, the correlation vanishes because of diffusion. Therefore, the  $\{i, j\}$ -th element of  $\mathbf{M}(\Delta T)$  at a long lag time becomes the product of the  $i$ th and  $j$ th points of the ensemble-averaged fluorescence decay curve:

$$M_{ij}^{\text{unc}} = \bar{I}(t^{(i)})\bar{I}(t^{(j)}). \quad (9)$$

One can obtain the correlated part of  $\mathbf{M}(\Delta T)$  by subtracting this uncorrelated part:

$$M_{ij}^{\text{cor}}(\Delta T) = M_{ij}(\Delta T) - M_{ij}^{\text{unc}}. \quad (10)$$

$\mathbf{M}^{\text{cor}}(\Delta T)$  does not contain any contributions from different molecules or uncorrelated backgrounds, because these contributions do not fluctuate in a correlated manner. It means that this separation of the correlated part enables us to treat  $\mathbf{M}^{\text{cor}}(\Delta T)$  as if it is built from a strict single-molecule experiment under an ideal condition, i.e., infinitesimally low concentration and no background scattering.

Figure 4 demonstrates the effect of subtraction of uncorrelated background [12]. The sample is a mixture of two fluorescent dyes, Cy3 and TMR (tetramethylrhodamine). Figure 4a shows the fluorescence decay curves of Cy3, TMR, and their mixture. The fluorescence lifetime of Cy3 is 0.18 ns and that of TMR is 2.4 ns. The fluorescence of the mixture solution shows a biexponential decay which corresponds to a sum of the TMR and Cy3 decay curves. Figure 4b is the 2D map of the uncorrelated background,  $\mathbf{M}^{\text{unc}}$ , and Fig. 4c shows that of the correlated part,  $\mathbf{M}^{\text{cor}}(\Delta T)$ , at  $\Delta T = 10\text{--}100 \mu\text{s}$ . A clear difference is seen between the shapes of these 2D maps. Namely, the correlated part lacks sharp ridges along the time-zero lines which are, in contrast, obvious in the uncorrelated part. These ridges represent the cross-correlation between the short lifetime component (Cy3) and the long lifetime component (TMR), so that their absence in the correlated part indicates that the cross-correlation between these components is zero. This cross-correlation should naturally be zero, because the sample is just a mixture of two independent

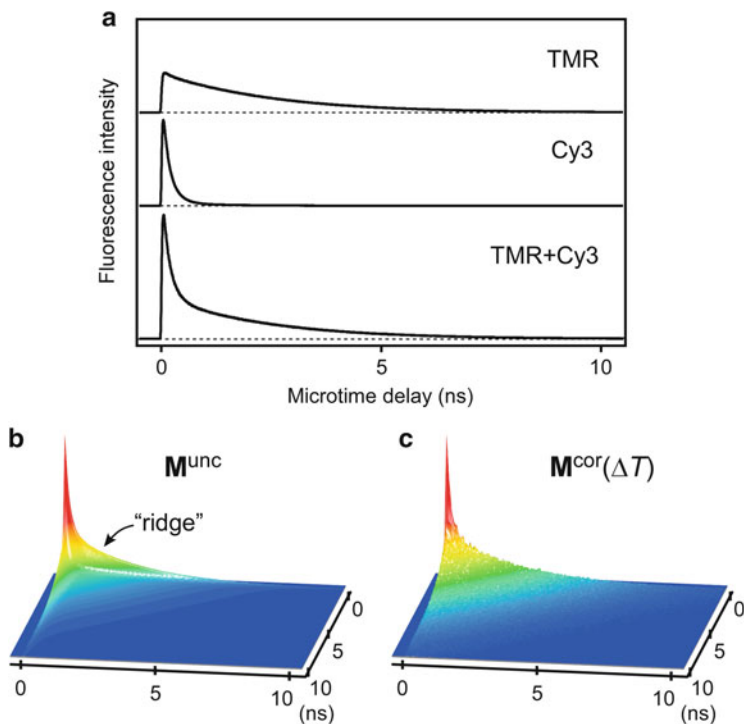


**Fig. 4** (a) Fluorescence decay curves of two fluorescent dyes (TMR and Cy3) and their mixture measured with the TCSPC method. (b, c) 2D correlation maps of the uncorrelated part (b) and the correlated part at  $\Delta T = 10\text{--}100\ \mu\text{s}$  (c) built from time-tagged TCSPC data of the mixture solution. Note that ridges are clearly visible in (b)

dyes. This consistency proves that the uncorrelated background is properly subtracted in this analysis. Thus, the correlated part can be regarded as an equivalent of the sum of the single-molecule correlation signals of TMR and Cy3.

### 3.3 Inverse Laplace Transform and Decomposition into Multiple Species

The next step is decomposition of  $M^{\text{cor}}(\Delta T)$  [11, 12]. When a sample consists of multiple species,  $M^{\text{cor}}(\Delta T)$  becomes the sum of contributions from these species. In such cases, one can decompose  $M^{\text{cor}}(\Delta T)$  into each contribution as follows to identify each species and to study their interconversion:

$$M_{ij}^{\text{cor}}(\Delta T) = \sum_{k,l} g_{kl}^{\text{cor}}(\Delta T) I_k(t^{(i)}) I_l(t^{(j)}). \quad (11)$$

Here,  $g_{kl}^{\text{cor}}(\Delta T)$  is the correlated part of the species-specific correlation function between  $k$  and  $l$ . If no exchange reaction occurs between different species, the corresponding cross-correlation ( $g_{kl}^{\text{cor}}(\Delta T)$ ,  $k \neq l$ ) becomes zero. On the other hand, if a reaction exchanging two species  $k$  and  $l$  takes place,  $g_{kl}^{\text{cor}}(\Delta T)$  starts appearing on the timescale of the reaction.

In practice, however, the decomposition of  $\mathbf{M}^{\text{cor}}(\Delta T)$  using Eq. (11) is not easy because the separation of fluorescence decay curves of different species in  $\mathbf{M}^{\text{cor}}(\Delta T)$  is not straightforward when reference data (i.e., the functional forms of  $I_i(t)$ 's) are not available. This complexity is reduced by considering the fluorescence lifetime of each species instead of the fluorescence decay curve. In general, one can represent the fluorescence decay curve of a certain species by using continuously distributed fluorescence lifetime,  $\tau$ , and corresponding amplitude,  $a(\tau)$ :

$$I(t) = \int_0^{\infty} a(\tau) \exp(-t/\tau) d\tau. \quad (12)$$

Then, one can rewrite  $\mathbf{M}^{\text{cor}}(\Delta T)$  as,

$$\begin{aligned} M_{ij}^{\text{cor}}(\Delta T) &= \sum_{k,l} g_{kl}^{\text{cor}}(\Delta T) \int_0^{\infty} a_k(\tau') \exp(-t^{(i)}/\tau') d\tau' \int_0^{\infty} a_l(\tau'') \exp(-t^{(j)}/\tau'') d\tau'' \\ &= \int_0^{\infty} \int_0^{\infty} \tilde{M}_{\tau'\tau''}(\Delta T) \exp(-t^{(i)}/\tau') \exp(-t^{(j)}/\tau'') d\tau' d\tau'', \end{aligned} \quad (13)$$

where we introduced a two-dimensional lifetime correlation map:

$$\tilde{M}_{\tau'\tau''}(\Delta T) = \sum_{k,l} g_{kl}^{\text{cor}}(\Delta T) a_k(\tau') a_l(\tau''). \quad (14)$$

$a(\tau)$  has well-separated peak(s) when each species has a well-defined fluorescence lifetime. It is also expected that  $\tilde{\mathbf{M}}(\Delta T)$  shows a clear peak pattern in a two-dimensional map which directly represents auto- and cross-correlations of the species in the sample. Therefore,  $\tilde{\mathbf{M}}(\Delta T)$  is much more suitable for intuitively interpreting the whole kinetics on the species basis. The conversion from  $I(t)$  to  $a(\tau)$  is formally equivalent to inverse Laplace transform (ILT) and the conversion  $\mathbf{M}^{\text{cor}}(\Delta T) \rightarrow \tilde{\mathbf{M}}(\Delta T)$  corresponds to two-dimensional ILT. Usually one needs a special procedure to perform ILT because it is known that ILT is numerically unstable. MEM (maximum entropy method) is sometimes employed for suppressing the numerical instability [17, 18]. As described in detail in a published paper [12], a MEM approach is used for this 2D ILT problem and  $\tilde{\mathbf{M}}(\Delta T)$  is obtained from  $\mathbf{M}^{\text{cor}}(\Delta T)$  in 2D FLCS.

The above-described procedure for obtaining  $\tilde{\mathbf{M}}(\Delta T)$  realizes 2D FLCS. The cross-correlation between different species ( $g_{kl}^{\text{cor}}(\Delta T)$ ,  $k \neq l$ ) appears in  $\tilde{\mathbf{M}}(\Delta T)$  map as an off-diagonal peak between two different lifetimes representing the species  $k$  and  $l$  (Eq. (14)). Therefore, by examining the  $\Delta T$ -dependence of the intensity of off-diagonal peaks, one can trace the temporal evolution of  $g_{kl}^{\text{cor}}(\Delta T)$ , which represents the equilibration process between the two species ( $k$  and  $l$ ).

Figure 5 shows an illustrative example of 2D FLCS [11]. Here, in order to exemplify the 2D FLCS analysis using well-defined parameters, a synthetic photon data was generated by kinetic Monte Carlo simulation. We assumed a two-state reaction model between states A and B with the forward rate constant  $k_f$  and the backward rate constant  $k_b$ , where  $k_f = k_b = (100 \mu\text{s})^{-1}$ . The fluorescence lifetimes of the states A and B were set at 1 and 5 ns, respectively. Figure 5a shows  $\mathbf{M}^{\text{cor}}(\Delta T)$  constructed from the simulated photon data for different lag times. One can see that the shape of the 2D correlation pattern changes with  $\Delta T$ , which are also evident in the slices of the 2D maps at different microtime values (Fig. 5a, bottom). This change reflects the interconversion between A and B which occurs during  $\Delta T$ . It can

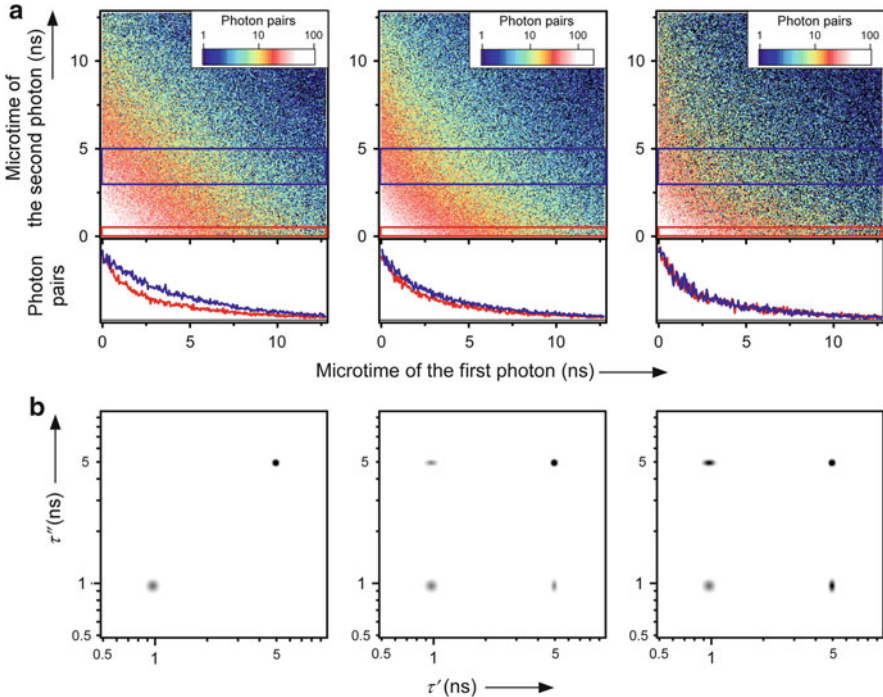


**Fig. 5** 2D FLCS applied to the synthetic photon data generated by kinetic Monte Carlo simulation. (a) The correlated part of the 2D map ( $\mathbf{M}^{\text{cor}}(\Delta T)$ ) at  $\Delta T = 0\text{--}10 \mu\text{s}$  (left),  $40\text{--}60 \mu\text{s}$  (center), and  $200\text{--}220 \mu\text{s}$  (right). The slices of these maps integrated over the colored rectangle regions are shown in the bottom with corresponding colors. (b) The converted 2D lifetime maps ( $\tilde{\mathbf{M}}(\Delta T)$ ) at  $\Delta T = 0\text{--}10 \mu\text{s}$  (left),  $40\text{--}60 \mu\text{s}$  (center), and  $200\text{--}220 \mu\text{s}$  (right)

be more clearly visualized by using 2D ILT that converts  $\mathbf{M}^{\text{cor}}(\Delta T)$  to  $\tilde{\mathbf{M}}(\Delta T)$  (Fig. 5b). In the converted 2D lifetime maps, one can clearly see isolated diagonal peaks, which correspond to the A ( $\tau = 1$  ns) and B states ( $\tau = 5$  ns). Absence of the cross peaks between these two states at the shortest lag time ( $\Delta T = 0\text{--}10$   $\mu\text{s}$ ) is a clear evidence of independence of these states. Subsequent gradual rise of the cross peaks reflects transformation between the two states, which accords with the adopted reaction model. This result exhibits that, by comparing 2D lifetime maps at different  $\Delta T$ , one can visualize the equilibration process between different species and determine its time constant in a species-specific manner.

### 3.4 Application: DNA Dynamics

Next, we show an application of 2D FLCS to the hairpin-forming DNA molecule that was examined in the previous section by lifetime-weighted FCS (Fig. 2) [12]. Here, in order to clarify the dynamics of DNA hairpin observed at  $\Delta T \sim 100$   $\mu\text{s}$ ,  $\mathbf{M}^{\text{cor}}(\Delta T)$  is built for three time regions encompassing this timescale (Fig. 6a). These  $\mathbf{M}^{\text{cor}}(\Delta T)$  exhibit  $\Delta T$ -dependent change. However, in contrast to the previous example, the change of  $\mathbf{M}^{\text{cor}}(\Delta T)$  is not very obvious and hence it is difficult to obtain physical insight directly from this 2D map. In this case, the conversion from  $\mathbf{M}^{\text{cor}}(\Delta T)$  to  $\tilde{\mathbf{M}}(\Delta T)$  by 2D ILT is very effective (Fig. 6b). In the 2D ILT analysis using MEM, we assumed three independent components that coexist in the sample. For these three components, MEM determined the fluorescence lifetime distribution,  $a_k(\tau)$ , and the auto- and cross-correlations,  $g_{kl}^{\text{cor}}(\Delta T)$  (Eqs. (13, 14)). The analysis was simultaneously performed on the three 2D maps shown in Fig. 6a, which enabled us to obtain a common set of  $a_k(\tau)$  that is independent of  $\Delta T$  (global analysis). The obtained  $a_k(\tau)$ 's ( $k = 1\text{--}3$ ) is shown in Fig. 6c. The observed peaks in  $\tilde{\mathbf{M}}(\Delta T)$  in the shortest  $\Delta T$  (Fig. 6b) correspond to the autocorrelation peaks of these three components. (Note that some components exhibit multi-exponential decays due to fast structural fluctuation, so that cross peaks appear in autocorrelation of these species.) Very importantly, one can find growth of new cross peaks in the second and third panels of Fig. 6b, as indicated by arrows. These cross peaks represent the origin of the  $\sim 100$   $\mu\text{s}$  dynamics of the DNA hairpin observed by the lifetime-weighted FCS (Fig. 2), and they correspond to the cross-correlation between the second ( $k = 2$ ) and the third ( $k = 3$ ) components in Fig. 6c. Based on the fluorescence decay measurements on control samples, the second and the third components were assigned to the open form and the closed form, respectively, whereas it was found that the first ( $k = 1$ ) component was due to the DNA molecule lacking an active acceptor dye [12]. Therefore, the observed dynamics is attributed to the interconversion between the open form and the closed form. On the other hand, any cross peaks between the first component and others are not observed. It is consistent with that the first component stems from a species without an active acceptor and hence its fluorescence lifetime does not change with the lag time  $\Delta T$ .

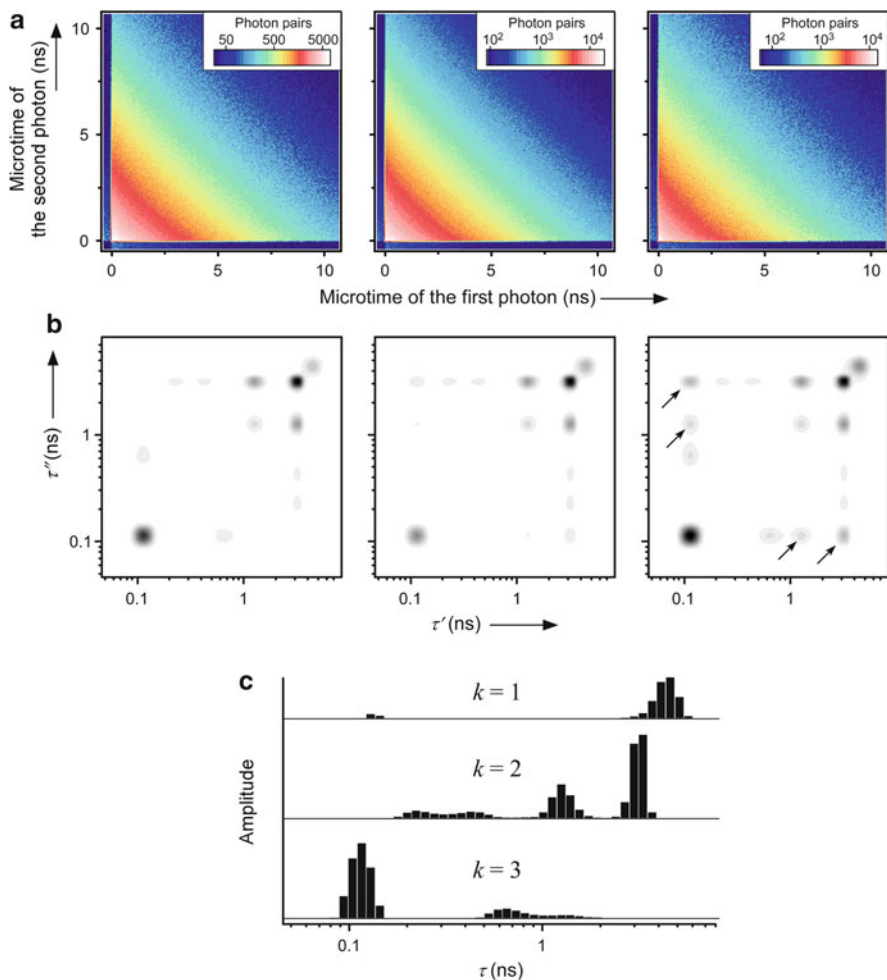
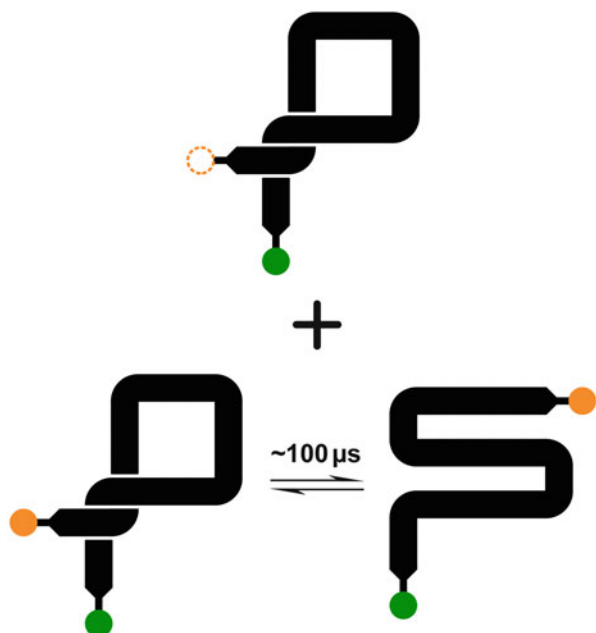


**Fig. 6** 2D FLCS of a DNA hairpin. **(a)** The correlated part of the 2D map ( $\mathbf{M}^{\text{cor}}(\Delta T)$ ) at  $\Delta T = 10\text{--}30\ \mu\text{s}$  (*left*),  $30\text{--}100\ \mu\text{s}$  (*center*), and  $100\text{--}200\ \mu\text{s}$  (*right*). **(b)** The converted 2D lifetime map ( $\tilde{\mathbf{M}}(\Delta T)$ ) at  $\Delta T = 10\text{--}30\ \mu\text{s}$  (*left*),  $30\text{--}100\ \mu\text{s}$  (*center*), and  $100\text{--}200\ \mu\text{s}$  (*right*). **(c)** Three independent components ( $a_k(\tau)$ ,  $k = 1\text{--}3$ ) that are extracted in the analysis. Their auto- and cross-correlations comprises 2D lifetime maps in **(b)**

Figure 7 summarizes the dynamics of the DNA hairpin concluded from this experiment. The dynamics of the hairpin DNA can be described by a two-state model between the open and closed forms, and the acceptor-inactive DNA coexists in the sample. The 2D FLCS was proven to be useful to obtain the species-specific correlation that can separate multiple species such as the open form, the closed form, and even inactive molecules in the sample, without any prior knowledge about each species.

**Fig. 7** A schematic picture of the dynamics of a DNA hairpin observed by 2D FLCS. *Green and orange circles* represent the donor (FAM) and acceptor (TAMRA) dyes, respectively. The closed form (*bottom left*) and the open form (*bottom right*) are equilibrated in  $\sim 100 \mu\text{s}$ , whereas an acceptor-inactive species (*top*) also exists in the sample solution



## 4 Photon Interval Analysis

So far, we have discussed how to quantify fluctuations of fluorescence lifetime using time-tagged TCSPC through two newly developed methods, i.e., lifetime-weighted FCS and 2D FLCS. In this section, we turn our attention to another way of using time-tagged TCSPC data, focusing on its local property. Instead of collecting every photon pairs found with a fixed time interval, we consider only photon pairs directly neighboring in the photon table, and examine the relationship between their microtimes and the time interval (Fig. 8a). Photon interval distribution is sometimes investigated by using the Hanbury Brown and Twiss setup [19] to study nanosecond photon correlations [20, 21], utilizing the definite relationship between the photon interval distribution and the intensity correlation function. Here, we present an application of photon interval analysis that incorporates microtime information, and show its usefulness for analyzing the timing instability problem of photon detectors [13].

Single photon avalanche photodiode (SPAD) is a photon detector commonly used in TCSPC experiments, particularly in single-molecule fluorescence lifetime measurements and fluorescence lifetime imaging (FLIM). A well-known drawback of SPADs is the counting-rate dependence of the shape and peak position of the instrument response function (IRF), which hampers accurate determination of the fluorescence lifetime. It has been claimed that this counting-rate dependence arises from the quenching circuit in SPADs [22]. In the following, this problem is analyzed by using the IRF data measured by time-tagged TCSPC, and an efficient calibration method is given [13].

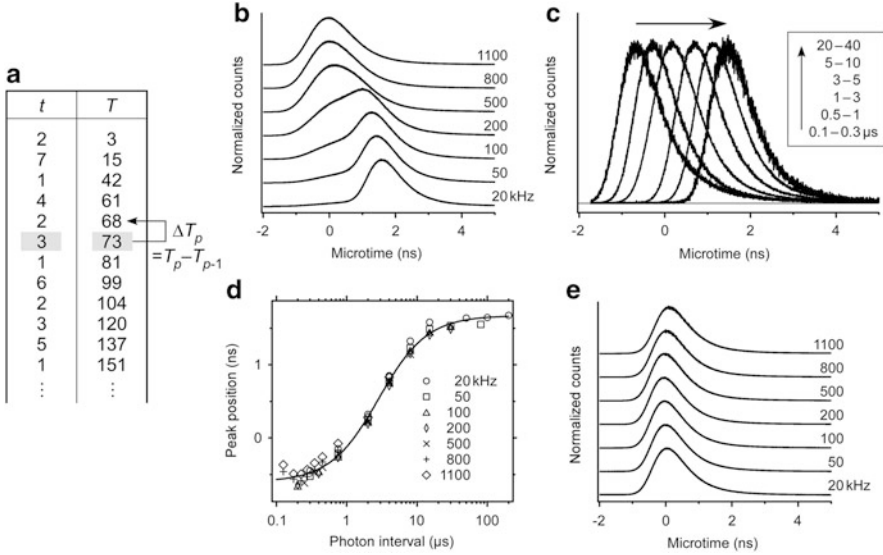


**Fig. 8** Photon interval analysis of time-tagged TCSPC data. **(a)** Definition of the photon interval of  $p$ th photon. **(b)** Counting-rate dependence of the IRF obtained with a SPAD. **(c)** IRF curves reconstructed from photons of selected  $\Delta T$  values. They demonstrate  $\Delta T$ -dependence of the IRF. **(d)**  $\Delta T$ -dependence of the peak position of the IRF measured at various counting rates. **(e)** Counting-rate dependence of the IRF after calibration

Figure 8b shows the counting-rate dependence of the IRF of a SPAD. These curves are obtained by building the microtime histogram of scattered photons of laser pulses with various intensities. The data clearly shows that the time profile of IRF drastically changes with the counting rate. To examine this timing instability in more detail, all the detected photons are classified according to the time interval with respect to the preceding photon using their macrotime information (Fig. 8a):

$$\Delta T_p = T_p - T_{p-1}. \quad (15)$$

$\Delta T$ -dependent IRF is evaluated by collecting photons that have common  $\Delta T$  values (Fig. 8c). The peak position of the IRF shows a monotonous shift with  $\Delta T$ , whereas the shape is mostly preserved. This implies that the counting-rate dependence observed in Fig. 8b is essentially due to  $\Delta T$ -dependent timing shift. The  $\Delta T$ -dependent peak position of IRF was measured at various counting rates and is plotted in Fig. 8d. It is clearly seen that the data measured with different counting rates overlap with each other and follow the same trend. This result leads us to conclude that the time interval,  $\Delta T$ , rather than the mean counting rate, is the factor that determines the timing instability.

If one analyzes the  $\Delta T$ -dependence of the mean delay time (Fig. 8d) in more detail, one may further obtain some insight into the underlying physics that causes the timing instability. However, even without going into the detail of the



mechanism, one can use this  $\Delta T$ -dependence for calibrating the counting-rate dependent timing shift [13]. Actually, the calibration curve is obtainable by fitting the  $\Delta T$ -dependent peak position of IRF (Fig. 8d) with an appropriate function. We used the Hill equation to fit the observed data (Fig. 8d, solid line). The microtime of any photons detected with the same detector can be calibrated using the same calibration curve. Figure 8e shows the calibrated IRF curves at various counting rates. The effect of the calibration is obvious, i.e., the shape and position of IRF become almost independent of the counting rate. This calibration allows us to obtain the best achievable time resolution in TCSPC experiments, particularly in applications such as FLIM where the counting rate largely fluctuates.

## 5 Concluding Remarks

In this chapter, we described two methods using time-tagged TCSPC, which have been recently developed to derive as much information as possible from the photon data collected. We note that these methods do not require any modification of the optical (microscopy) setup of a standard TCSPC, because they are purely numerical algorithms. However, these methods can extract information that is usually hidden under seemingly random fluctuations. Even though the structure of time-tagged TCSPC data is rather simple, we believe that the obtainable knowledge from the data has not been fully exploited yet. Therefore, there exist vast possibilities to extend the usage of time-tagged TCSPC for various applications.

## References

1. Becker W (2005) Advanced time-correlated single photon counting techniques. Springer series in chemical physics, vol 81. Springer, Heidelberg
2. Eggeling C, Fries JR, Brand L, Günther R, Seidel CAM (1998) Monitoring conformational dynamics of a single molecule by selective fluorescence spectroscopy. *Proc Natl Acad Sci U S A* 95:1556–1561
3. Palo K, Brand L, Eggeling C, Jaeger S, Kask P, Gall K (2002) Fluorescence intensity and lifetime distribution analysis: toward higher accuracy in fluorescence fluctuation spectroscopy. *Biophys J* 83:605–618
4. Yang H, Xie XS (2002) Probing single-molecule dynamics photon by photon. *J Chem Phys* 117:10965–10979
5. Boehmer M, Wahl M, Rahn H-J, Erdmann R, Enderlein J (2002) Time-resolved fluorescence correlation spectroscopy. *Chem Phys Lett* 353:439–445
6. Gregor I, Enderlein J (2007) Time-resolved methods in biophysics. 3. Fluorescence lifetime correlation spectroscopy. *Photochem Photobiol Sci* 6:13–18
7. Kapusta P, Wahl M, Benda A, Hof M, Enderlein J (2007) Fluorescence lifetime correlation spectroscopy. *J Fluoresc* 17:43–48
8. Kapusta P, Macháň R, Benda A, Hof M (2012) Fluorescence lifetime correlation spectroscopy (FLCS): concepts, applications and outlook. *Int J Mol Sci* 13:12890–12910

9. Ishii K, Tahara T (2010) Resolving inhomogeneity using lifetime-weighted fluorescence correlation spectroscopy. *J Phys Chem B* 114:12383–12391
10. Ishii K, Tahara T (2012) Extracting decay curves of the correlated fluorescence photons measured in fluorescence correlation spectroscopy. *Chem Phys Lett* 519–520:130–133
11. Ishii K, Tahara T (2013) Two-dimensional fluorescence lifetime correlation spectroscopy. 1. Principle. *J Phys Chem B* 117:11414–11422
12. Ishii K, Tahara T (2013) Two-dimensional fluorescence lifetime correlation spectroscopy. 2. Application. *J Phys Chem B* 117:11423–11432
13. Otsu T, Ishii K, Tahara T (2013) Note: simple calibration of the counting-rate dependence of the timing shift of single photon avalanche diodes by photon interval analysis. *Rev Sci Instrum* 84:036105
14. Lakowicz JR (2006) Principles of fluorescence spectroscopy, 3rd edn. Springer, New York
15. Yang H, Xie XS (2002) Statistical approaches for probing single-molecule dynamics photon-by-photon. *Chem Phys* 284:423–437
16. Burstyn HC, Sengers JV (1983) Time dependence of critical concentration fluctuations in a binary liquid. *Phys Rev A* 27:1071–1085
17. Livesey AK, Brochon JC (1987) Analyzing the distribution of decay constants in pulse-fluorimetry using the maximum entropy method. *Biophys J* 52:693–706
18. Brochon JC (1994) Maximum entropy method of data analysis in time-resolved spectroscopy. *Methods Enzymol* 240:262–311
19. Hanbury Brown R, Twiss RQ (1956) Correlation between photons in two coherent beams of light. *Nature* 177:27–29
20. Berglund AJ, Doherty AC, Mabuchi H (2002) Photon statistics and dynamics of fluorescence resonance energy transfer. *Phys Rev Lett* 89:068101
21. Nettels D, Gopich IV, Hoffmann A, Schuler B (2007) Ultrafast dynamics of protein collapse from single-molecule photon statistics. *Proc Natl Acad Sci U S A* 104:2655–2660
22. Rech I, Labanca I, Ghioni M, Cova S (2006) Modified single photon counting modules for optimal timing performance. *Rev Sci Instrum* 77:033104